The Effects of Ice Habit on Simulated Orographic Snowfall

LUCAS J. STERZINGER[a] AND ADELE L. IGEL[a]

[a] *Department of Land, Air and Water Resources, University of California, Davis, Davis, California*

(Manuscript received 21 October 2020, in final form 5 April 2021)

ABSTRACT: Many factors are at play in determining the amount and distribution of mountain snowfall predicted by weather models; among them is the influence of assumed ice habit. Ice habit is necessarily greatly simplified in microphysics schemes and uncertainty remains in how best to model ice processes. In this study we simulate a Sierra Nevada snowfall event driven by an extratropical cyclone in February 2014. We have simulated the storm with four fixed-habit types as well as with an ice habit scheme that is variable in time and space. In contrast to some previous studies, we found substantially smaller sensitivity of total accumulated precipitation amount and negligible changes in spatial distribution to the ice habit specification. The reason for smaller sensitivity seems to be linked to strong aggregation of ice crystals in the model. Nonetheless, while changes in total accumulated precipitation were small, changes in accumulated ice hydrometeors were larger. The variable-habit simulation produced up to 37% more ice precipitation than any of the fixed-habit simulations with an average increase of 14%. The variable-habit simulation led to a maximization of ice growth in the atmosphere and, subsequently, ice accumulation at the surface. This result points to the potential importance of accounting for the time and space variation of ice crystal properties in simulations of orographic precipitation.

KEYWORDS: Cloud microphysics; Ice crystals; Cloud parameterizations; Regional models; Mountain meteorology

1. Introduction

Snowfall in mountainous regions is important for several reasons; in many water-scarce places, melting mountain snow is a substantial part of the yearly water budget. In California, for example, the water from melting snowpack accounts for 30% of the state's water needs (California Department of Water Resources 2019). The elevation the snow falls at is important, as lower-elevation snow will melt sooner in the year and may impact water planning and damming operations. The high albedo of snow also acts as a regulator of near-surface temperature, and many studies (Rangwala and Miller 2012, and references therein) have shown that the melting of mountain snow can spur a feedback loop (melting snow lowers albedo, surface warming increases, which leads to faster melting) that causes higher elevations to warm more rapidly than lower regions. For example, the Colorado Rocky Mountains were observed to be warming 0.05°C decade^{-1} faster annually than the average Northern Hemisphere land surface, and 0.25°C decade^{-1} faster in the springtime months (Rangwala and Miller 2012). As such, it is important for both numerical weather prediction (NWP) and climate modeling systems to be able to accurately represent spatial and temporal coverage of snowpack in mountainous areas. This accuracy is necessarily tied to the representation of in-cloud processes that generate ice crystals, and as such the knowledge of ice-phase physics and the treatment of ice in a particular model's microphysics scheme is important.

The Sierra Nevada mountains provide a somewhat uniquely important case: in the north the mountains are located along the border between California and Nevada, meaning any ice that melts on the lee side can flow into Nevada's Great Basin; a shift in snow from leeward/windward could affect which state can claim the water rights. In the southern Sierras, the location of snowpack determines whether the water will flow into the Sacramento and San Joaquin river delta or southward into the Los Angeles basin. The watershed in which snowpack will melt is important to water managers in California and Nevada, who have to plan for needs in historically water-scarce areas.

The physics of atmospheric ice, and their representation in models, are more complicated than their liquid counterpart. First, the formation of ice crystals occurs through several mechanisms, many of which are not well understood (e.g., Cantrell and Heymsfield 2005; Murray et al. 2012). These mechanisms include heterogeneous freezing pathways involving ice nuclei, as well as secondary ice production caused by complex fragmentation during collision, riming (e.g., Hallett and Mossop 1974), freezing, and sublimation.

Second, even a relatively simple property like the habit (shape) of an ice crystal has wide-ranging effects on its behavior. Ice habit primarily depends on the ambient temperature and supersaturation with respect to ice (Nakaya 1954; Kobayashi 1957; Hallett and Mason 1958; Fletcher 1962; Bailey and Hallett 2009) and has profound effects on its growth rate (e.g., Ono 1970; Takahashi and Fukuta 1988; Takahashi et al. 1991; Chen and Lamb 1994; Fukuta and Takahashi 1999), fall speed (e.g., Locatelli and Hobbs 1974), and radiative scattering properties (e.g., Yang and Liou 1998). Fall speed in particular is an important factor in determining the spatial distribution of orographic snowfall. Strong horizontal transport that often occurs with wintertime mountainous snowfall means that as ice crystals fall through the atmosphere, they are advected upslope. The fall speed of a particle then is a primary determinant of how far downwind the particle is advected before settling on the surface. If two crystals were dropped simultaneously under these conditions, we would expect the slower-falling crystal to accumulate farther upslope.

Corresponding author: Lucas Sterzinger, lsterzinger@ucdavis.edu

DOI: 10.1175/JHM-D-20-0253.1

Third, ice crystals commonly aggregate to form loose clusters of crystals, and rime as they fall through supercooled liquid water. Both of these processes create ice hydrometeors which can vary widely in shape and density, which in turn makes generalizing their properties difficult. Recent studies (Dunnavan et al. 2019; Karrer et al. 2020) have shown that the shape and density of aggregates (and therefore their fall speed) depend on the properties of the individual monomers that make up an aggregate.

The complexity of atmospheric ice must be simplified in models. Most modern operational, large-domain models use bulk microphysics (BMP) schemes, which typically calculate the mass mixing ratio and perhaps the number concentration (in double-moment schemes) for a wide variety of hydrometeor species, oftentimes cloud water, rain, cloud ice, snow, graupel and/or hail. The complexities of ice processes are simplified in order to fit the framework of BMPs. Many BMP schemes neglect ice habit entirely [e.g., Hong et al. 2004 (WSM6); Thompson et al. 2004; Morrison et al. 2009] and instead assume spherical snow with a constant density. However, many observational studies (Locatelli and Hobbs 1974; Mitchell et al. 1990; McFarquhar and Black 2004) have concluded that this assumption is not representative of most situations. More recent schemes, such as Thompson et al. (2008) (the default in WRF v4.0's "CONUS" physics suite), reject the constant density, spherical snow assumption and instead use a more representative mass-diameter relationship that effectively allows for density to decrease as the snow size increases. While a single-category variable density method certainly allows for an increase in ice variability, it would only be able to distinguish between similarly shaped crystals (e.g., plates being a higher density version of a dendrite). A recent study by Naeger et al. (2020), which evaluated several BMP schemes' performance simulating an atmospheric river snowfall event over the Olympic Mountains, showed that the spherical-snow assumption in the Morrison et al. (2009) scheme generated larger than observed snow particles and weak melting rates, resulting in slower fall speeds below the melting layer; the nonspherical snow of Thompson et al. (2008) allowed for faster melting and a more realistic representation of fall speeds below the melting layer.

There have been some efforts to include some of the more complex ice properties into cutting-edge BMP schemes. Notably, the Predicted Particle Properties (P3; Morrison and Milbrandt 2015) and Ice-Spheroids Habit Model with Aspect-Ratio Evolution (ISHMAEL; Jensen et al. 2017) schemes have limited the partitioning of ice into defined, fixed categories with separate power laws and instead modify the coefficients and powers [e.g., α and β in the mass–diameter relationship $m(D) = \alpha D^{\beta}$] dynamically and continuously as an ice particle rimes (and, in ISHMAEL, as it grows via deposition). Both P3 and ISHMAEL improve upon traditional ice representation by allowing for variation in rimed-ice density; ISHMAEL further predicts the shape of ice's major and minor axes allowing for variance in the axis ratio, yielding more physical representation of shape-dependent processes such as depositional growth, riming, and fall speed. Tsai and Chen (2020) have designed a triple-moment bulk scheme with adaptive habits similar to P3 and ISHMAEL. Special attention was given to the influence of ice crystal shape and density on processes like aggregation and riming. This scheme reclassifies ice-type hydrometeors; pristine ice particles are able to grow only by deposition and have no upper size limit, removing the typical microphysics scheme transition from small cloud ice to larger snow.

These schemes show promise in improving the representation of ice in BMP schemes; Naeger et al. (2020) found that the prognostic treatment of riming within P3's single ice category allowed for enhanced rimed mass, more accumulation, and, as a result, more accurate precipitation predictions. Jensen et al. (2018) used the ISHMAEL scheme to simulate a wintertime atmospheric river in the Pacific Northwest that produced significant orographic snowfall. They found that the better representation of ice fall speeds improved the spatial distribution of mountainous snow over traditional bulk schemes when compared to observations. ISHMAEL was also used to simulate lake effect snow in Jensen et al. (2020) and, while the study did not directly compare ISHMAEL to traditional schemes, the authors concluded by hypothesizing that schemes like P3 and ISHMAEL may be less sensitive to changes in riming that occur when increasing model resolution than traditional schemes. Two-dimensional sensitivity tests of a squall line using the Tsai and Chen (2020) scheme showed that the detailed treatment of ice shape and density, as well as the addition of a third predicted moment, had significant impacts on the microphysical structure of the storm resulting in weaker precipitation at the surface.

While the importance of ice properties is well recognized, the impact of ice habit on orographic snowfall has not typically been investigated directly. Colle and Zeng (2004) found that by slowing the sedimentation rate of snow, 20%–30% more snow mass was produced, mainly due to increased accretion of cloud and rainwater that created more graupel and reduced melting. The authors also found that a decrease in fall velocity caused a decrease in lower elevation precipitation by 10%–20% and an increase of 10%–60% in higher-elevation precipitation due to increased advection and decreased melting. While their work did not directly look at ice habit, sedimentation fall speeds are one of the main properties directly impacted by habit.

Similarly, Woods et al. (2007) universally changed the mass–diameter [$m(D)$] and velocity–diameter [$v(D)$] relationships of snow to behave as various habits (spheres, dendrites, needles, and columns; see Table 2 in Woods et al. 2007). Changing $v(D)$ alone caused significant horizontal shifts in orographic precipitation accumulation. Changing both $v(D)$ and $m(D)$ resulted in more accumulated precipitation in all experiments and caused significant shifts in spatial accumulation with the slow-falling dendrites accumulating heavily upslope compared to the other habit experiments (similar to results seen in Colle and Zeng 2004).

On the other hand, Gaudet et al. (2019) found very little sensitivity of precipitation accumulation to ice habit treatment with an adaptive habit model (Harrington et al. 2013; the basis for ISHMAEL) on a mesoscale lake effect snow event over Lake Ontario and western New York. They found that allowing nonspherical growth increased precipitation by only 1.6%–2.3%. It is unclear why the sensitivity is so much smaller

than in Colle and Zeng (2004) or Woods et al. (2007). One possible reason is that Gaudet et al. (2019) examined lake effect snow rather than orographic snow. Another is that the schemes tested in Woods et al. (2007) and Colle and Zeng (2004) were both single-moment, predicting only the mass mixing ratio for most species whereas Gaudet et al. (2019) used a fully double-moment scheme that predicts both mass and number.

In this study, we further investigate the effect that ice habit has on mountainous snowfall. Unlike in the two mountain precipitation studies discussed above (Colle and Zeng 2004; Woods et al. 2007), we will use a full double-moment microphysics scheme and simultaneously modify a suite of habit-related properties to test the impact of habit type on snowfall. We will also investigate the consequences of diagnosing habit such that it can vary in time and space. Specifically, we pose the following questions:

- What is the sensitivity of orographic snowfall accumulation and spatial distribution to comprehensive changes in ice habit?
- How are microphysical process rates modified as a result of changing the habit type?

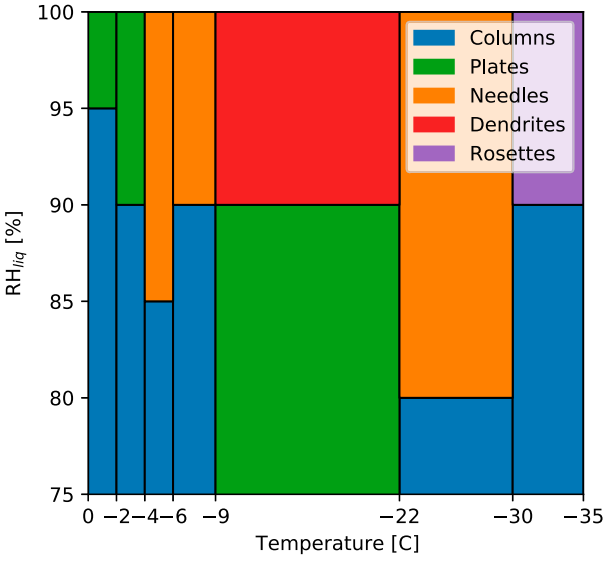

FIG. 1. RAMS diagnosed ice habit categories, values taken from Fletcher (1962). The diagnosed habit is dependent on the temperature and the relative humidity with respect to liquid water.

2. Methodology

a. Model description

To evaluate the sensitivity of orographic snowfall to ice crystal habit, a set of simulations was run with the Regional Atmospheric Modeling System (RAMS; Cotton et al. 2003). RAMS has been previously used to simulate other mesoscale wintertime orographic snow events (Poulos et al. 2002; Meyers et al. 2003; Saleeby and Cotton 2005). The RAMS model uses a bin-emulating double-moment bulk microphysics scheme that predicts the mass mixing ratio and number concentration for eight hydrometeor species: cloud water, drizzle, rain, pristine ice, snow, aggregates, graupel, and hail (Walko et al. 1995; Meyers et al. 1997; Saleeby and Cotton 2004; Saleeby and van den Heever 2013). Pristine ice and snow are both single crystal categories that are distinguished by crystal size whereas the aggregates category represents ice crystal clusters. The graupel and hail categories represent rimed ice and are distinguished by their density.

Within the snow and pristine ice categories, the RAMS microphysics scheme has two broad options for ice habit treatment: 1) The user specifies a fixed-habit type for all pristine ice and snow crystals that does not vary in space or time. Options include plates, needles, dendrites, columns, and bullet rosettes. 2) RAMS diagnoses the crystal habit based on the environmental temperature and relative humidity with respect to liquid water (Meyers et al. 1997), with threshold values based on theory from Fletcher (1962) and visualized in Fig. 1. The habit classifications affect the $m(D)$ and $v(D)$ relationships (shown in Fig. 2), and capacitance (a parameter in the vapor growth equation that depends on the size and shape) of the ice crystal. These properties affect the deposition/sublimation, riming, aggregation, and sedimentation rates. For each call to the microphysics routine, the model diagnoses the ice habit for a particular grid cell, and assigns the above properties as necessary. The model does not track habits as ice is advected and sedimented between grid cells; the ice particles thus change habit instantaneously according to the environment of the current cell. This behavior is unrealistic and we would expect smooth transitions between or even mixtures of ice habits that reflect the history of the crystals in the real atmosphere. A possible side effect of this treatment is an instantaneous slowing or quickening of fall speed as crystals fall into grid boxes with different habit designations. Nonetheless, this approach does allow for spatial and temporal variation of ice habit in ways that many models do not allow at all. We will use both ice habit treatment options in this study.

In our discussion of results, a few of the hydrometeor categories will be grouped together for simplicity. Pristine ice and snow (hereafter "ice crystals") have a habit assigned to them by the model. Aggregates are formed by the collision and collection of ice crystals, and do not have a habit type. Graupel and hail are also combined (hereafter "rimed ice") and also do not have a habit.

b. Model setup

For this study, RAMS is used to simulate a typical wintertime atmospheric river that impacted Northern California and the Sierra Nevada mountains from 6 to 10 February 2014. The model was run with a large domain of 4500 km × 4500 km with 15-km spacing, and a two-way nested grid over the Sierra Nevada mountains of 925 km × 700 km with 5-km spacing. A snapshot of model simulated integrated water vapor (shaded colors) and sea level pressure (contours) is shown in Fig. 3a where the plotted area represents the large domain, and the red box represents the nested domain (which is zoomed in on Fig. 3b, with 500-m topographic contours). The larger domain extends west into the Pacific Ocean in order to properly

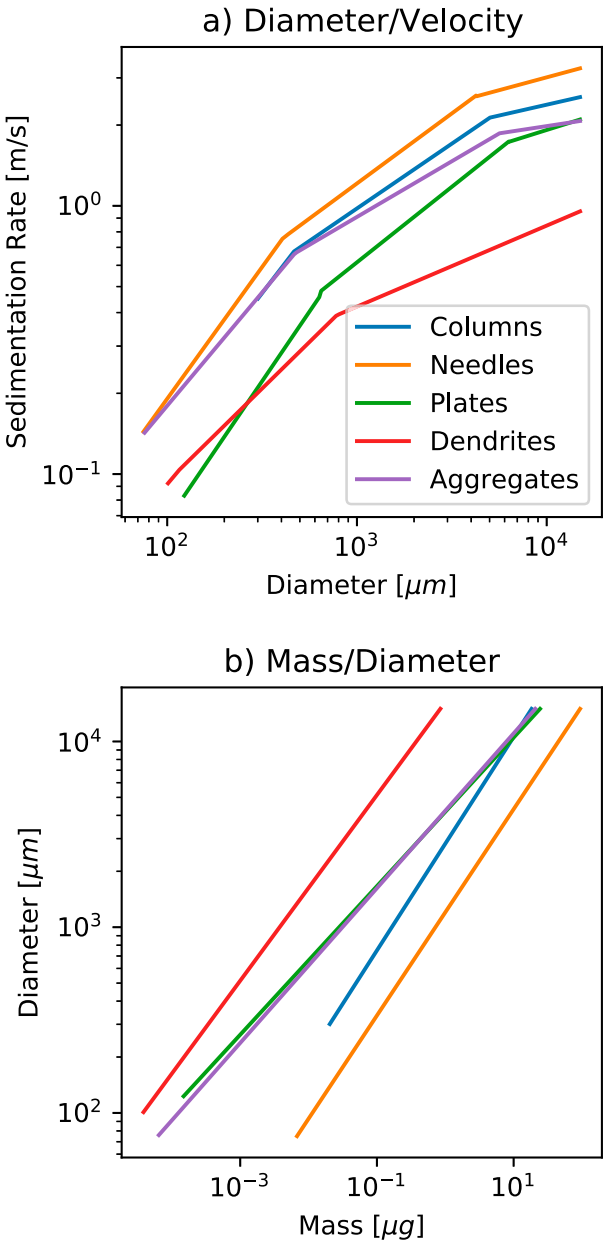

FIG. 2. RAMS (a) diameter–velocity and (b) mass–diameter relationships for the simulated habit categories and aggregates.

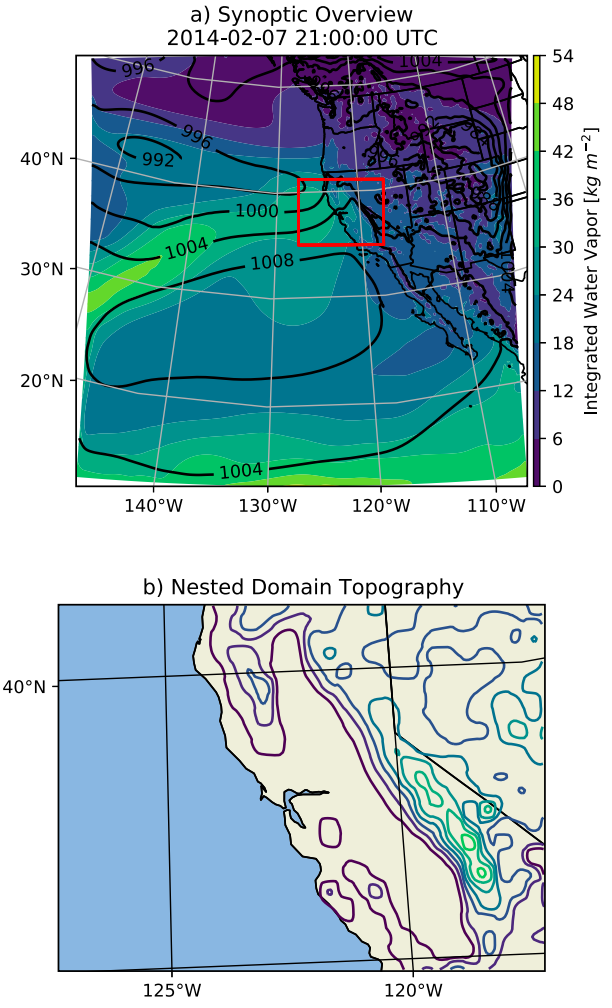

FIG. 3. (a) Synoptic overview of the storm, with sea level pressure (contoured; hPa) and integrated water vapor (shaded; kg m^{-2}) at 2100 UTC 7 Feb 2014. The nested domain used in this study is shown in red. (b) The nested domain with topographic contours at 500-m intervals.

capture the low pressure system and associated atmospheric river of this storm. For both domains, 60 terrain-following vertical levels were used with a maximum altitude of 29 km. The vertical spacing increases from 100 m at the surface to a maximum of 1000 m at the top of the domain. The coarse domain had an integration time step of 30 s, and the nested domain had an integration time step of 15 s.

The model was initialized at 1200 UTC 5 February 2014 and was run until 0000 UTC 11 February 2014. Initial and boundary conditions were provided by the North American Regional Reanalysis (NARR; Mesinger et al. 2006) at 3-hourly intervals. NARR was also used for analysis nudging where temperature, wind, and water mass near domain boundaries are relaxed toward NARR values with a 15-min time scale. Output for the nested domain was written to files at every hour of simulation time.

An initial simulation was run in which the diagnostic habit option within the RAMS microphysics scheme was used (DIAG). A suite of four additional simulations were also run; these simulations were identical to the control simulation except that a fixed single habit type was used instead of using the diagnostic habit scheme. All simulations are listed in Table 1. The specific habits were chosen because they represent the four most common ice habits produced during the diagnostic simulation.

c. *Comparison to observations*

The accumulated precipitation from DIAG was qualitatively compared against the NOAA Advanced Hydrologic Precipitation Dataset (AHPS; Lawrence et al. 2003). AHPS

TABLE 1. Model experiments and acronyms.

Expt	Habit	Description
DIAG	Diagnostic	Habit diagnosis
COL	Columns	Long round column-shaped crystals
NED	Needles	Longer and thinner than columns
PLA	Plates	Flat hexagonal plates with no branching
DEN	Dendrites	Flat hexagonal crystals with branches

is a gridded, 4 km × 4 km precipitation dataset that provides daily precipitation totals at 1200 UTC (which is the standard end of the hydrologic day). AHPS uses WSR-88D NEXRAD radar-derived hourly precipitation measurements, which are then adjusted based on reported rain gauge values.

Figures 4a and 4b shows a comparison between the total accumulated precipitation in DIAG and the AHPS radar-estimated precipitation for a period that extends 12 h past the simulation period. RAMS does well at representing the magnitude and location of the precipitation maximum in the Sierra Nevada mountains, though the modeled precipitation is slightly narrower and extends farther south along the Sierra Nevada mountain range.

The storm simulated in this study affected the Sierra Nevada mountains in three distinct waves over 5 days as indicated by the three time periods of rapid accumulated precipitation increases in Fig. 4c. The vertical lines indicate subjectively determined transitions from one wave to the next. The characteristics of the three waves will be discussed in more detail below.

d. *Data analysis*

To facilitate the analysis, terrain-aligned means are used. For each east–west cross section in the nested model domain, the highest point on the mountain range was found. Data 150 km to the west and 75 km to the east of that point were taken and composited along the north/south axis. This allows for a better analysis of various processes relative to the crest of the mountain range (shown below in section 3), as well as a rudimentary east/west watershed separation. All further analysis in this paper is done using the terrain-aligned mean domain.

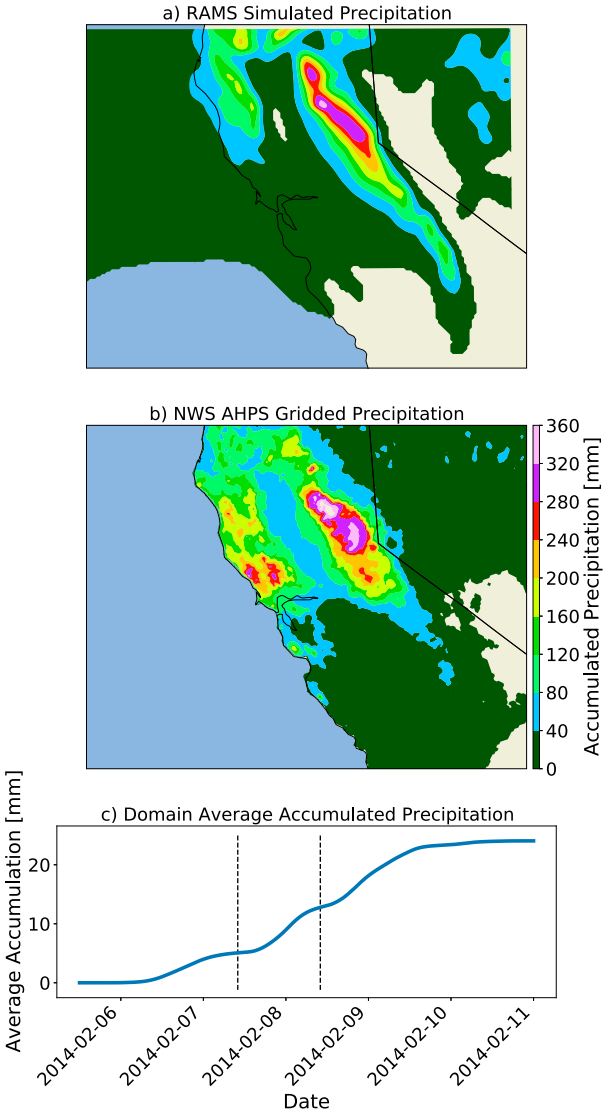

FIG. 4. Comparison between total precipitation in (a) DIAG and (b) NWS AHPS observed precipitation. (c) The modeled average accumulated precipitation is also shown, with dashed lines denoting the boundaries between the three waves of the storm. Wave boundaries are at 1000 UTC 7 Feb and 1000 UTC 8 Feb.

3. Results and discussion

a. *Accumulated precipitation*

Figure 5 shows both the accumulation of ice-type (Fig. 5a) and all hydrometeors (ice + liquid, Fig. 5b). The first wave was the coldest and produced the most frozen precipitation. As the storm progressed, it became warmer and more of the precipitation fell as rain. For the first two waves of the storm, the melting level was, on average, at or below the crest of the mountains. The third wave was warm enough that the mean melting level was above the average mountain crest, causing significantly less accumulated ice than during the other two waves, even though it produced the most total precipitation.

DIAG consistently produced the most total precipitation of all simulations. Among the fixed-habit experiments, no particular ice habit simulation consistently produced the most precipitation, although PLA tended to be among the highest and NED tended to be among the lowest. Total accumulations vary by 6% on average between simulations and at most 12.4%, while ice accumulations vary by 14% on average and at most 37%. These values are smaller than those observed in Colle and Zeng (2004) and Woods et al. (2007) but larger than those of Gaudet et al. (2019).

Figure 6 shows the fraction of accumulated ice contributed by ice crystals, aggregates, and rimed ice during each of the three waves. As a reminder, "ice crystals" represents the hydrometeor categories with habit information (pristine ice and snow) and "rimed ice" represents both graupel and hail. In all three waves of the storm, the accumulated ice was dominated

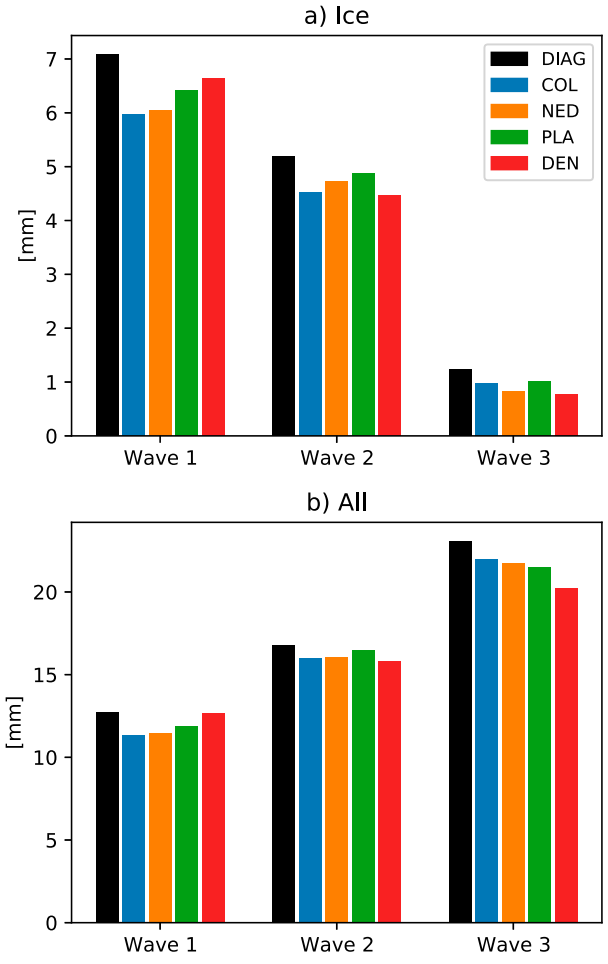

FIG. 5. The mean snow water equivalent depth in millimeters analyzed over the Sierra Nevada mountains for each wave of the storm. Mean depth is given for (a) all ice type hydrometeors (ice crystals, rimed ice, and aggregates) and (b) all hydrometeors (ice crystals, rimed ice, aggregates, drizzle, and rain).

by aggregates and rimed ice. This is unsurprising; ice crystals often collide to form aggregates, and riming is expected when there is a large amount of supercooled liquid water present. The DEN simulation, for example, produces the most aggregates and the least amount of rimed ice, fitting well with our understanding of dendrites' high aggregation efficiency. The ice habit treatment caused changes of about 10% in the accumulation fractions of rimed ice and aggregates. Larger relative changes occurred in the accumulation fractions of the less-prevalent ice crystals with shifts of near 50% between some habit experiments. The results in Figs. 5 and 6 together show that even though there is minimal accumulation of ice crystals, the ice crystal habit specification did have a moderate impact on the type of and total precipitation at the surface.

b. *Spatial distribution of precipitation*

One aspect of mountain snowfall that warrants attention is the distribution of accumulated snow across various watersheds. A basic watershed study can be set up by analyzing the distribution of accumulated snow between the leeward (eastern) and windward (western) side of the mountains. This is easily done with the terrain-aligned mean framework described previously in section 2d. Figure 7 shows the fractional east/west distribution for all ice-type hydrometeors. In general, much more precipitation is expected to fall on the windward side than on the leeward side, as is shown. The east/west fraction of all ice species varies slightly between experiments, but the amounts that have shifted are only 1%–5% of the total ice accumulation.

We further examine the spatial distribution of precipitation by analyzing it in relation to elevation. Figure 8 shows the fraction of total precipitation (Figs. 8a–c) and fraction of ice precipitation (Figs. 8d–f) in 200-m elevation bins. For all precipitation, simulations are in agreement except for a slight divergence at high altitudes, which accounts for a small fraction (0.1%–1%) of the total precipitation. Conversely, for ice-type precipitation, the largest differences between the simulations occur at the lowest elevations, where the smallest amount of ice accumulates. Overall, there are negligible changes to the spatial distribution of precipitation.

Colle and Zeng (2004) analyzed the effects of a slower ice crystal fall speed on the total precipitation (ice + liquid). They found that a decrease in fall speed correlated to a decrease in lower-elevation precipitation by 10%–20% and an increase in the upper-elevation and leeside precipitation by 10%–60%. Figures 8d–f show that no significant shifts in precipitation occurred at altitudes with any meaningful ice accumulation, suggesting that there was little shift in elevation between habit experiments. Total snow amounts varied between experiments (as shown in Fig. 5a), which does show the effect that habit has on snow accumulations. However, we were unable to find evidence in our data of the elevation shifts in accumulation as described in Colle and Zeng (2004).

It is worth noting that single-moment scheme used in Colle and Zeng (2004) was only modified for the $v(D)$ and not the $m(D)$ relationship in their experiments. However, as described above, RAMS habit assignment affects the $v(D)$, $m(D)$, and capacitance of the ice crystals. Importantly, the capacitance affects ice growth rates, which could further complicate comparison between the results shown here and the $v(D)$ tests done by Colle and Zeng (2004). RAMS' scheme is also double-moment, predicting mass and number concentrations for all hydrometeors rather than the single-moment scheme in Colle and Zeng (2004), which prescribed a number concentration for all hydrometeors. Woods et al. (2007) performed sensitivity studies while modifying both $v(D)$ and $v(D) + m(D)$ and found the inclusion of $m(D)$ modifications increases the total precipitation in all habit experiments, and shifts precipitation upslope for their dendrite experiment. The DEN experiment in the results shown here do not show a shift up- or downslope compared to the other experiments, most likely due to the transfer of pristine ice and snow to nonhabit tracking frozen hydrometeor categories such as aggregates and graupel.

c. *In-cloud processes*

To explain the above observations, a detailed look at the in-cloud processes is needed. As discussed in the

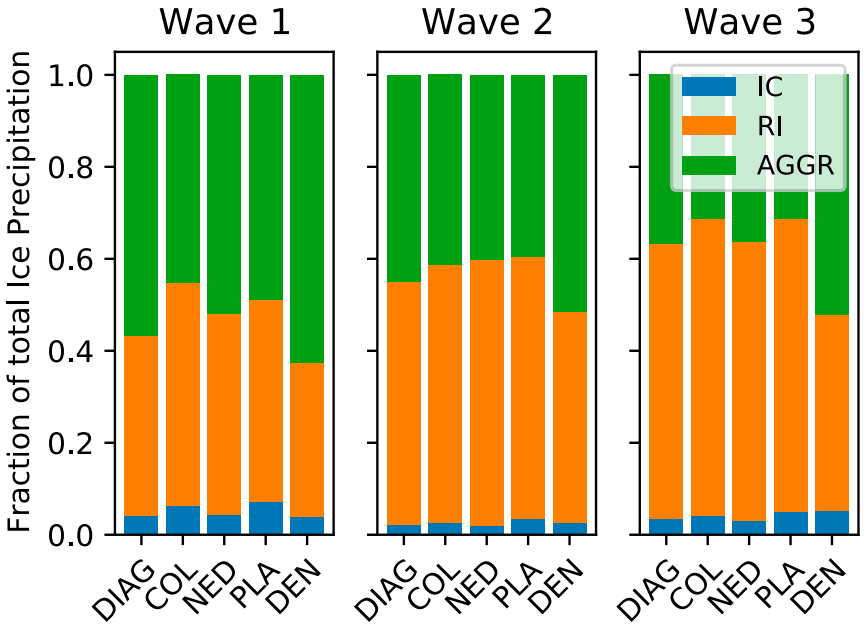

FIG. 6. Accumulated ice crystals (IC), aggregates (AGGR), and rimed ice (RI) during each of the three waves. Amounts are shown as the fraction of total accumulated ice-type precipitation for each wave.

description of the RAMS model, the habit diagnosis affects the $m(D)$, $v(D)$ relationships as well as the capacitance, which together modify deposition/sublimation, riming, and collection (aggregation) rates. As such, all variations seen in Figs. 5–7 must fundamentally link back to these processes.

We aim to explain two phenomena seen in the results above:

- The change in the relative amounts of accumulated hydrometeors in each experiment (Figs. 6–8); specifically why the DIAG simulation produced the most total precipitation.
- The lack of changes in the spatial distribution of precipitation (Figs. 7 and 8).

As discussed previously, the storm precipitated in three distinct waves. For the sake of brevity and simplicity we will focus our

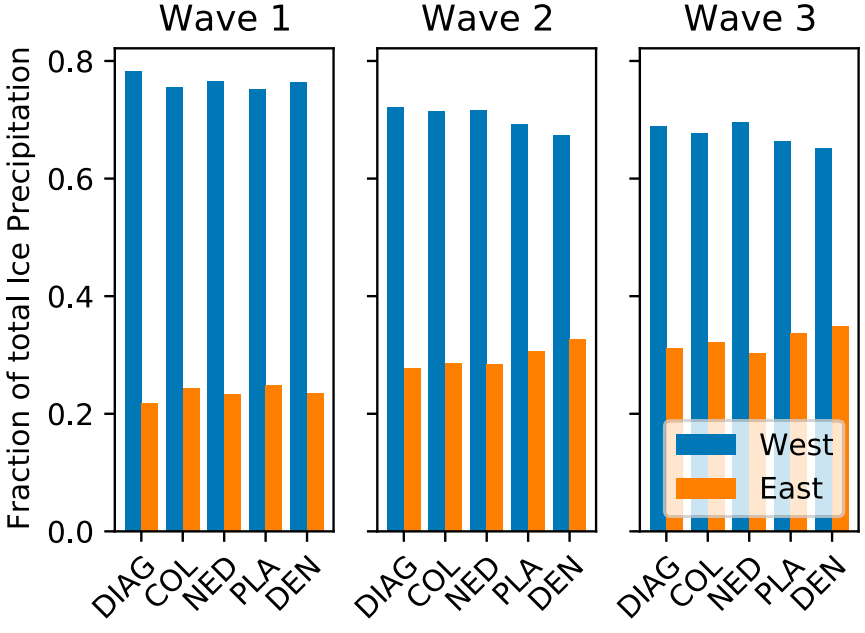

FIG. 7. Fraction of accumulated ice-type precipitation that fell on the western or eastern slope of the mountains for all three waves.

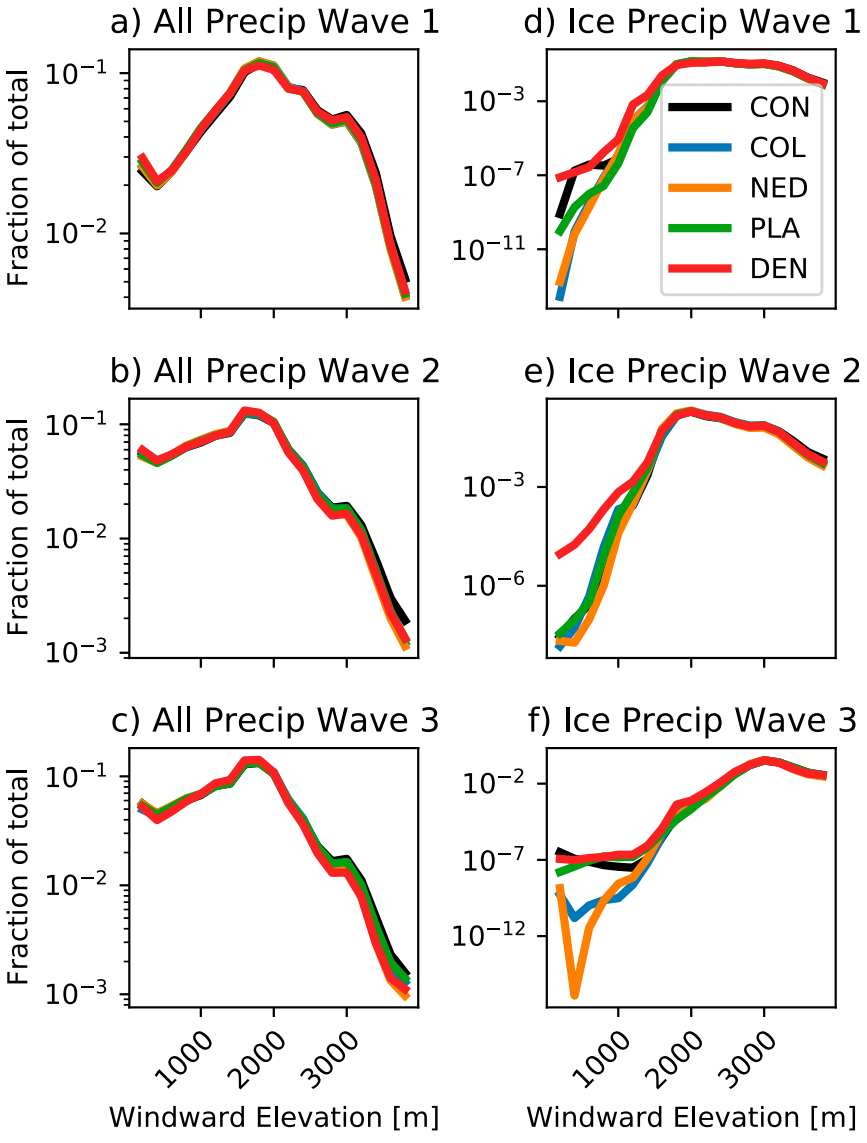

FIG. 8. Spatial distribution of (a)–(c) all accumulated hydrometeors and (d)–(f) only ice-type hydrometeors during all three waves of the storm, taken with elevation bins of 200 m. Amounts shown as a fraction of the total precipitation for that specific simulation.

analysis on the second of these waves. The qualitative results shown below for wave 2 are also valid for waves 1 and 3 (not shown). As in the previous sections, all analysis is performed over the terrain-aligned grid.

To understand the differences between the variable and fixed-habit experiments, knowledge of the vertical habit distribution in DIAG is needed. Figure 9 shows the vertical distribution of ice habit in DIAG as a fraction of total grid boxes with ice present. Above 6 km, columns were the dominant diagnosed species, accounting for 90% or more of the diagnosed ice habits. Below 6 km, the habit type is a strong function of height with layers of plates, dendrites, and needles. Most importantly for the analysis below, dendrites are the dominant habit in a narrow layer between about 4 and 4.5 km.

1) MASS MIXING RATIOS

Figure 10 shows vertical profiles of mean mass mixing ratios in wave 2 for ice crystals, aggregates, rimed ice, and cloud water. Around 2.5 km and below, ice mass (Figs. 10a,b,d) is dominated by rimed ice and aggregates whereas ice crystals are dominant above 6 km. This vertical distribution of ice mass aligns well with the results shown in Fig. 6 where aggregates and rimed ice made up the majority of accumulated ice-type hydrometeors. This shift in the dominant ice type at the lower levels arises primarily from ice crystals aggregating and riming,

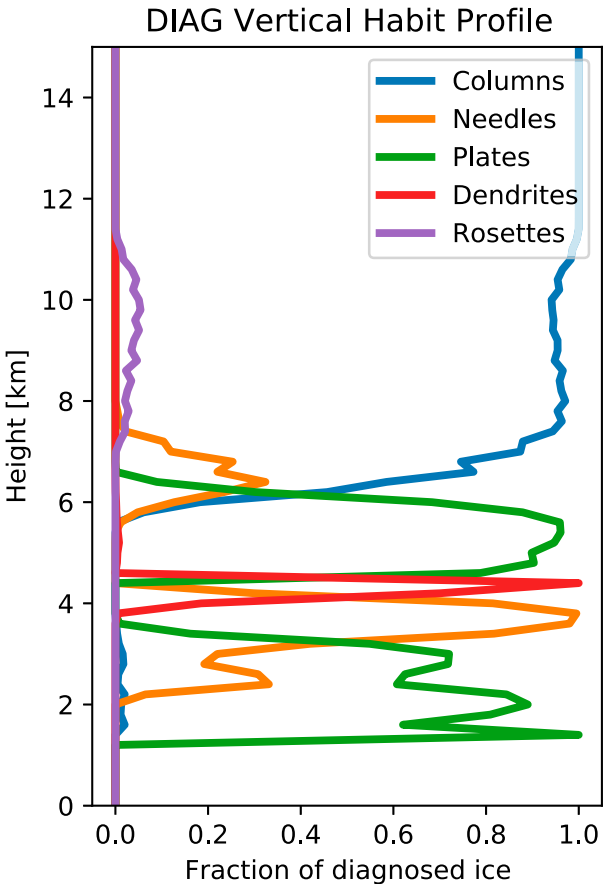

FIG. 9. Fraction of the terrain-aligned domain with ice present that were assigned a particular habit in wave 2; heights are kilometers above sea levels.

removing mass from the ice crystal categories and adding mass to aggregates and rimed ice, respectively (Figs. 11b,c).

DIAG has the highest mass of aggregates and rimed ice at nearly all levels, which is consistent with the results shown in Fig. 5 in which DIAG has the highest amount of accumulated precipitation of all simulations. DIAG also has average or above average ice crystal mixing ratios at all levels. The COL, NED, and PLA ice crystal and aggregates mixing ratios, when summed together, are similar (Fig. 10c). Rimed ice mixing ratios are also similar for DIAG, COL, NED, and PLA. On the other hand, DEN has about 50% less rimed mass than any other simulation. DEN also stands out as having the least aggregate mass and relatively low ice crystal mass (the reason behind this will be explained further in the next section). These results are consistent with Fig. 5 where DEN has the lowest total ice precipitation during wave 2 and with Fig. 6 where DEN was shown to have the lowest fraction of accumulated rimed ice. The significant decrease in rimed ice mass in DEN is likely explained by the low cloud water content at the same level in Fig. 10e, as well as increased DEN fall speeds (discussed in following section). The available cloud water is around 50% less for DEN than for the rest of the experiments at the 3-km level. A possible explanation for this is that the high depositional growth of DEN ice crystals limited the vapor available to cloud water for condensational growth and/or occurred at the expense of cloud water via the Wegener–Bergeron–Findeisen (WBF) process in which ice crystals grow and reduce the relative humidity to below saturation and cause liquid drops to evaporate (Wegener 1911; Bergeron 1935; Findeisen 1938). This lack of cloud water would inhibit riming and allow more aggregates to accumulate on the surface (as in Fig. 6 where DEN had the highest fraction of accumulated aggregates).

The lack of a shift in the spatial distribution of precipitation is very likely linked to the dominance of aggregates and rimed ice in the atmosphere up to about 5 or 6 km. Since these ice types do not have a habit, they fall with the same mass–velocity relationship in all experiments (see Fig. 2). This may be unphysical behavior as aggregate properties have been shown to depend on the properties of the monomers. It is also possible that RAMS is overaggressive in its aggregation, and that this over aggregation is acting as an equalizer in the fall speeds of various ice habits. Regardless, we would expect to see greater shifts in the spatial distribution in cases where ice crystals are more dominant such that their habit-dependent fall speeds were the primary means of sedimenting ice to the surface.

2) IN-CLOUD PROCESSES

To investigate the causes for the shifts in hydrometeor masses seen in Fig. 10, the processes that control the transfer of mass between these categories must be examined. A selection of these processes (ice depositional growth, aggregation, riming, cloud condensational growth, aggregate depositional growth, and aggregate fall speed) is shown in Fig. 11.

The ice depositional growth rate (Fig. 11a) varies by habit, with the highest rates occurring in DEN and the lowest occurring in COL and NED. DIAG typically has similar depositional growth rates to PLA except between about 4 and 5 km where the rates are more similar to those in DEN. Ice crystal depositional growth is particularity high for DEN at all levels, and this high rate affects the amount of water vapor available for condensation onto cloud droplets. This impact is visible in Fig. 10d where the cloud liquid water content for the DEN experiment is noticeably smaller than for the rest of the simulations, as well as in the low cloud droplet growth rates in Fig. 11d. Water vapor being used for ice growth rather than liquid growth decreases the amount of liquid available for riming and explains the higher fraction of accumulated aggregates in Fig. 6 in DEN.

As mentioned in the previous section, DEN stands out for having the least amount of aggregate mass (Fig. 10b) while also having the highest aggregation rates of all simulations (Fig. 11b). The DEN simulation initiated aggregation at a higher altitude than any other simulation and the resulting aggregates were larger than those of the other simulations. Consequently, DEN aggregates were larger but less numerous compared to the other simulations (not shown). This results in less aggregate mass in DEN, as these particles fell out quickly (Fig. 11f) and thus did not collectively grow by deposition as quickly as in the other simulations (Fig. 11e).

In DIAG, dendrites are only diagnosed in a very small section of the atmosphere around 4 km (Fig. 9). As such, depositional growth

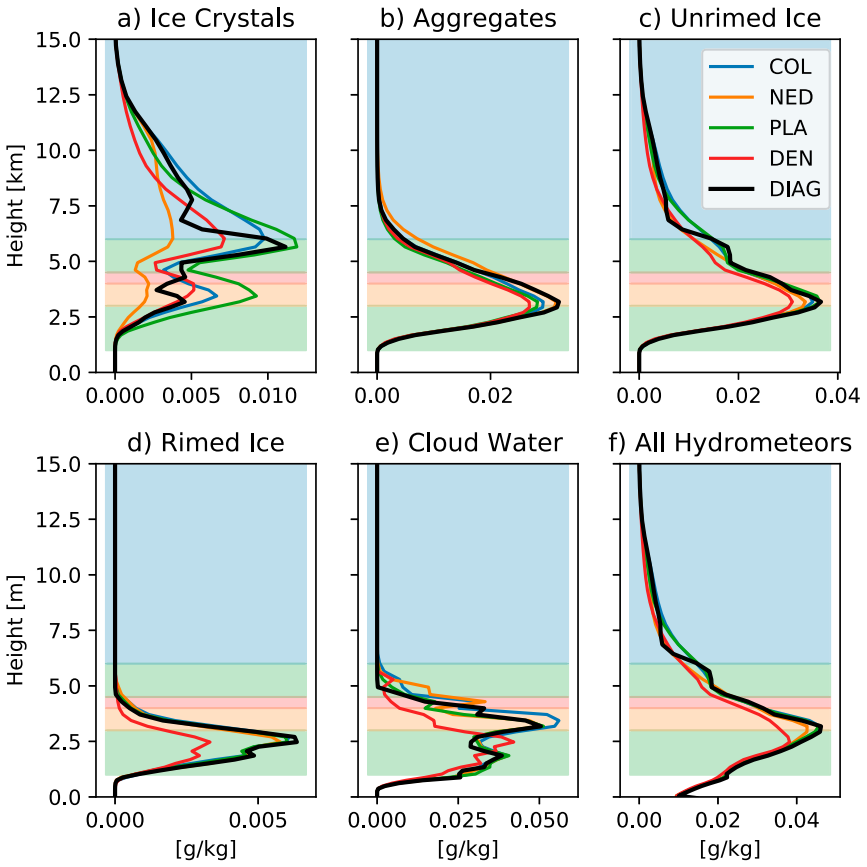

FIG. 10. Mean profiles of mass mixing ratio during wave 2 for (a) ice crystals, (b) aggregates, (c) unrimed ice [(a) + (b)], (d) rimed ice, (e) cloud water, and (f) all hydrometeors (rain/drizzle, ice crystals, aggregates, and rimed ice) for all fixed-habit experiments (colored lines) and DIAG (black line); heights are in kilometers above sea level. The shaded background corresponds to the dominant habit diagnosed by DIAG, as shown in Fig. 9 (green = plates, orange = needles, red = dendrites, blue = columns).

is high in DIAG at these altitudes. However, since this high depositional growth rate only occurs in a narrow range of altitudes, water vapor is not as depleted as much for DIAG as it is for DEN. This is noticeable in the cloud water mass in Fig. 10d, where cloud water in DIAG is only slightly reduced compared to the rest of the experiments while cloud water in DEN is noticeably lower. This means that DIAG maximizes ice crystal growth, while also maintaining high riming rates (unlike DEN). While this maximization is, of course, case dependent, it demonstrates possible consequences of spatially varying ice habit and its effect on cloud processes and precipitation. While the fixed-habit experiments either maximize ice deposition or riming (but not both), DIAG is able to maximize both processes, thereby accumulating more ice precipitation on the ground than any of the fixed-habit experiments.

Examination of the other two waves (not shown) reveals that the DEN simulation consistently rimed less compared to the rest of the experiments. This lack of riming reduces an important source of ice mass for the DEN experiment and is likely part of the reason that DEN had lower ice precipitation than the other habit experiments in wave 2 (Fig. 5). Wave 1 was the coldest and had the lowest freezing level (not shown), with less liquid water available for riming than in other waves. In this instance, ice production is dominated by depositional growth rather than riming, and DEN has the highest total ice accumulation. The reverse is true for wave 3, the warmest wave, and in which DEN has the lowest ice precipitation. This indicates that riming rates are indirectly dependent on habit (e.g., Takahashi and Fukuta 1988) and that riming is a critical process for transferring moisture from the atmosphere to accumulating precipitation.

4. Conclusions

In this study, we examined the sensitivity of orographic snowfall to ice crystal habit. We chose a case that represented a typical wintertime atmospheric river storm over the California Sierra Nevada mountains and ran a suite of experiments with a fixed ice habit [either columns (COL), plates (PLA), needles (NED), or dendrites (DEN)], as well as a simulation that used RAMS' diagnostic habit scheme (DIAG).

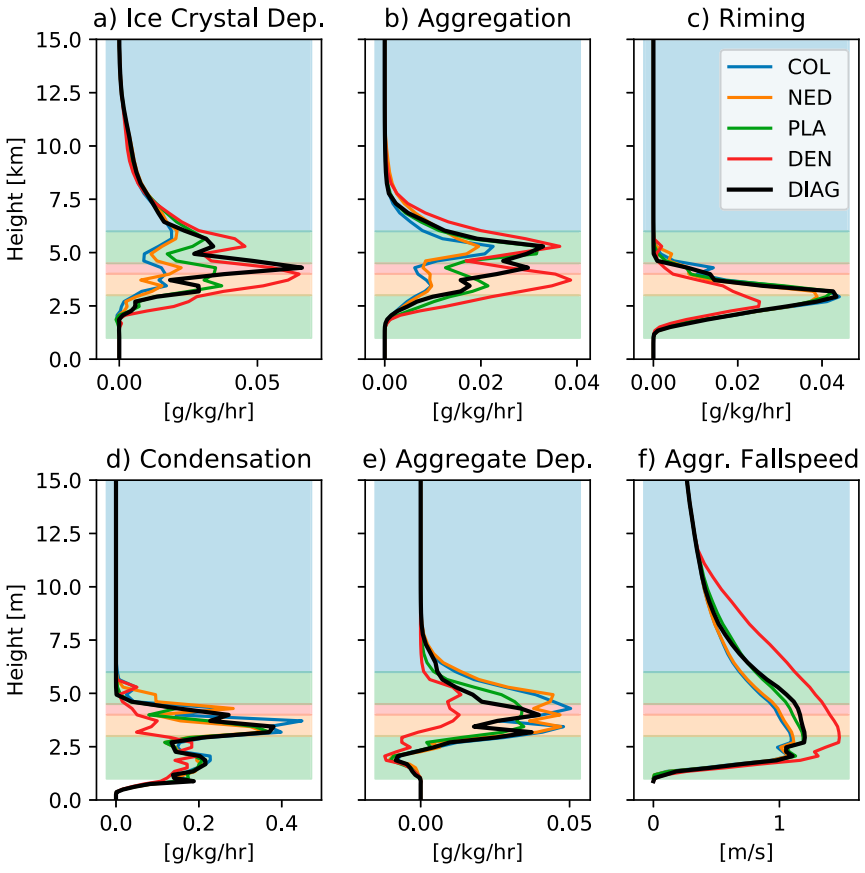

FIG. 11. As in Fig. 10, but for the processes (a) ice crystal deposition, (b) aggregation, (c) riming, (d) cloud condensational growth, (e) aggregate depositional growth, and (f) aggregate precipitation rate. Note that (f) has units of $\mathrm{m\,s^{-1}}$, while the rest of the panels have units of $\mathrm{g\,kg^{-1}\,h^{-1}}$.

DIAG consistently had the highest values of accumulated ice and total precipitation, and the differences in accumulation between DIAG and fixed-habit simulations were often larger than differences solely between fixed-habit simulations. While DIAG was comprised primarily of the four habits chosen for the experimental simulations, it was able to produce, on average, 14% more ice over the Sierra Nevada mountains than any of the individual experiment simulations with a maximum of 37% between DIAG and DEN in the third wave. This is a smaller sensitivity than reported in recent orographic snowfall studies that investigated habit (Colle and Zeng 2004; Woods et al. 2007), but larger than a recent study by Gaudet et al. (2019) examining sensitivity of lake-effect snowfall to ice habit. Our results show that the accumulated snowfall was often more sensitive to allowing variable habits than uniform changes to fixed-habit properties.

In addition to total accumulation, the spatial distribution of accumulated snowfall is of particular interest. We found minimal changes in the fractional amount of accumulated precipitation on the windward and leeward sides of the mountain range as well as minimal changes as a function of elevation among habit experiments. We believe that these results are primarily due to the fairly quick transfer of habit-type (ice crystals and snow) ice to non-habit-type ice (rimed and aggregated ice), which are treated the same across experiments. Minimal shifts in accumulated precipitation by elevation differs from what has been reported in Colle and Zeng (2004) and Woods et al. (2007); though these studies were analyzing different cases with different modeling setups than what was done in this study. Aggregates and rimed ice categories individually follow the same set of mass–diameter and velocity–diameter relationships, so a transfer of ice mass to these categories effectively masks any further habit sensitivity. Recent studies (Dunnavan et al. 2019; Karrer et al. 2020) have shown that aggregate properties depend on the properties of individual monomers, but this is not an aspect of ice crystal habit that is represented in the RAMS bulk scheme. The RAMS model may be overaggressive in its aggregation and a study examining various aggregation efficiencies effects on habit sensitivity would be a natural follow-up to the work presented here.

An investigation of the vertical structure of hydrometeor mass and process rates indicates that ice habit has a significant effect on ice crystal mass and ice-related process rates. In particular, the DEN simulation stands out as behaving differently than the other fixed-habit experiments. DEN produces significantly less rimed ice than the other experiments, due to a

lack of cloud water at the levels in which peak riming occurred. We find this to be primarily caused by the increased ice growth of the dendrite habit which effectively removed available water vapor for cloud droplets. The DIAG simulation, which was able to switch between habits depending on the environmental factors used by RAMS' habit diagnosis system (temperature and relative humidity w.r.t. liquid, Fig. 1), was able to use the high dendritic growth rates to its advantage. Since dendrites were only diagnosed in a small section of the atmosphere, the DIAG ice crystals were able to grow quickly at this level, but not enough to cause a substantial decrease in cloud water content. This allowed for a maximization of ice mass production in DIAG due to the habit diagnosis system implemented in the model. This diagnosis system allows for better physical representation of ice in the atmosphere and, as shown here, can have significant effects on surface ice accumulation. It is, however, not without its limitations. The instantaneous change of ice habit as ice falls or is advected between grid cells may result in unrealistic slowing or quickening that may influence results. However, all simulations showed similar spatial distribution of accumulation along the slope of the mountain, so this change in fall speed likely did not significantly affect the results.

While we recognize that this ice production maximization is very much case specific, the changes in accumulated ice precipitation demonstrate the potential importance of having a habit-diagnostic or habit-prognostic microphysics scheme. The results show that the modeled accumulated snowfall is more sensitive to the ability to vary habits in space and time than to uniform changes to properties of single-habit simulations. Had less ice mass been transferred to the singular aggregate category, a greater sensitivity to habit type may have been observed. We argue that, with the rapid increase in computing affordability, special attention should be given to ice habit in regional and climate models in order to more physically represent ice processes and likely more accurate snowfall amounts.

Acknowledgments. This project was supported by start-up funds for A. Igel from the University of California, Davis. We would like to acknowledge high-performance computing support from Cheyenne (doi:10.5065/D6RX99HX) provided by NCAR's Computational and Information Systems Laboratory, sponsored by the National Science Foundation. We thank the three anonymous reviewers for their time providing valuable comments on this paper.

Data availability statement. Model output data from this study can be found at http://farm.cse.ucdavis.edu/~lsterzin/ice_habit_simulations/ or by emailing the author at lsterzinger@ucdavis.edu

REFERENCES

Bailey, M. P., and J. Hallett, 2009: A comprehensive habit diagram for atmospheric ice crystals: Confirmation from the laboratory, AIRS II, and other field studies. *J. Atmos. Sci.*, **66**, 2888–2899, https://doi.org/10.1175/2009JAS2883.1.

Bergeron, T., 1935: On the physics of clouds and precipitation. *Proc. Fifth Assembly U.G.G.I.*, Lisbon, Portugal, U.G.G.I, 156–180, https://ci.nii.ac.jp/naid/10024028214/.

California Department of Water Resources, 2019: Latest snow survey finds water-rich snowpack. California Dept. of Water Resources, accessed 22 July 2019, https://water.ca.gov/News/News-Releases/2019/February/Latest-Snow-Survey-Finds-Water-Rich-Snowpack.

Cantrell, W., and A. Heymsfield, 2005: Production of ice in tropospheric clouds: A review. *Bull. Amer. Meteor. Soc.*, **86**, 795–808, https://doi.org/10.1175/BAMS-86-6-795.

Chen, J.-P., and D. Lamb, 1994: The theoretical basis for the parameterization of ice crystal habits: Growth by vapor deposition. *J. Atmos. Sci.*, **51**, 1206–1222, https://doi.org/10.1175/1520-0469(1994)051<1206:TTBFTP>2.0.CO;2.

Colle, B. A., and Y. Zeng, 2004: Bulk microphysical sensitivities within the MM5 for orographic precipitation. Part I: The Sierra 1986 event. *Mon. Wea. Rev.*, **132**, 2780–2801, https://doi.org/10.1175/MWR2821.1.

Cotton, W. R., and Coauthors, 2003: RAMS 2001: Current status and future directions. *Meteor. Atmos. Phys.*, **82**, 5–29, https://doi.org/10.1007/s00703-001-0584-9.

Dunnavan, E. L., Z. Jiang, J. Y. Harrington, J. Verlinde, K. Fitch, and T. J. Garrett, 2019: The shape and density evolution of snow aggregates. *J. Atmos. Sci.*, **76**, 3919–3940, https://doi.org/10.1175/JAS-D-19-0066.1.

Findeisen, W., 1938: Kolloid-meteorologische Vorgänge bei Neiderschlags-bildung. *Meteor. Z.*, **55**, 121–133.

Fletcher, N. H., 1962: *The Physics of Rainclouds*. University Press, 389 pp.

Fukuta, N., and T. Takahashi, 1999: The growth of atmospheric ice crystals: A summary of findings in vertical supercooled cloud tunnel studies. *J. Atmos. Sci.*, **56**, 1963–1979, https://doi.org/10.1175/1520-0469(1999)056<1963:TGOAIC>2.0.CO;2.

Gaudet, L. C., K. J. Sulia, F. Yu, and G. Luo, 2019: Sensitivity of lake-effect cloud microphysical processes to ice crystal habit and nucleation during OWLeS IOP4. *J. Atmos. Sci.*, **76**, 3411–3434, https://doi.org/10.1175/JAS-D-19-0004.1.

Hallett, J., and B. J. Mason, 1958: The influence of temperature and supersaturation on the habit of ice crystals grown from the vapour. *Proc. Roy. Soc. London*, **247A**, 440–453, https://doi.org/10.1098/rspa.1958.0199.

——, and S. C. Mossop, 1974: Production of secondary ice particles during the riming process. *Nature*, **249**, 26–28, https://doi.org/10.1038/249026a0.

Harrington, J. Y., K. Sulia, and H. Morrison, 2013: A method for adaptive habit prediction in bulk microphysical models. Part I: Theoretical development. *J. Atmos. Sci.*, **70**, 349–364, https://doi.org/10.1175/JAS-D-12-040.1.

Hong, S.-Y., J. Dudhia, and S.-H. Chen, 2004: A revised approach to ice microphysical processes for the bulk parameterization of clouds and precipitation. *Mon. Wea. Rev.*, **132**, 103–120, https://doi.org/10.1175/1520-0493(2004)132<0103:ARATIM>2.0.CO;2.

Jensen, A. A., J. Y. Harrington, H. Morrison, and J. A. Milbrandt, 2017: Predicting ice shape evolution in a bulk microphysics model. *J. Atmos. Sci.*, **74**, 2081–2104, https://doi.org/10.1175/JAS-D-16-0350.1.

——, ——, and ——, 2018: Impacts of ice particle shape and density evolution on the distribution of orographic precipitation. *J. Atmos. Sci.*, **75**, 3095–3114, https://doi.org/10.1175/JAS-D-17-0400.1.

——, P. T. Bergmaier, B. Geerts, H. Morrison, and L. S. Campbell, 2020: Sensitivity of convective cell dynamics and microphysics to model resolution for the OWLeS IOP2b lake-effect snowband. *Mon. Wea. Rev.*, **148**, 3305–3328, https://doi.org/10.1175/MWR-D-19-0320.1.

Karrer, M., A. Seifert, C. Siewert, D. Ori, A. V. Lerber, and S. Kneifel, 2020: Ice particle properties inferred from aggregation modelling. *J. Adv. Model. Earth Syst.*, **12**, e2020MS002066, https://doi.org/10.1029/2020MS002066.

Kobayashi, T., 1957: Experimental researches on the snow crystal habit and growth by means of a diffusion cloud chamber. *J. Meteor. Soc. Japan*, **35A**, 38–47, https://doi.org/10.2151/jmsj1923.35A.0_38.

Lawrence, B. A., M. I. Shebsovich, M. J. Glaudemans, and P. S. Tilles, 2003: Enhancing precipitation estimation capabilities at National Weather Service field offices using multi-sensor precipitation data mosaics. *19th Int. Conf. on Interactive Information Processing Systems*, Seattle, WA, Amer. Meteor. Soc., 15.1, https://ams.confex.com/ams/annual2003/techprogram/paper_54867.htm.

Locatelli, J. D., and P. V. Hobbs, 1974: Fall speeds and masses of solid precipitation particles. *J. Geophys. Res.*, **79**, 2185–2197, https://doi.org/10.1029/JC079i015p02185.

McFarquhar, G. M., and R. A. Black, 2004: Observations of particle size and phase in tropical cyclones: Implications for mesoscale modeling of microphysical processes. *J. Atmos. Sci.*, **61**, 422–439, https://doi.org/10.1175/1520-0469(2004)061<0422:OOPSAP>2.0.CO;2.

Mesinger, F., and Coauthors, 2006: North American Regional Reanalysis. *Bull. Amer. Meteor. Soc.*, **87**, 343–360, https://doi.org/10.1175/BAMS-87-3-343.

Meyers, M. P., R. L. Walko, J. Y. Harrington, and W. R. Cotton, 1997: New RAMS cloud microphysics parameterization. Part II: The two-moment scheme. *Atmos. Res.*, **45**, 3–39, https://doi.org/10.1016/S0169-8095(97)00018-5.

——, J. S. Snook, D. A. Wesley, and G. S. Poulos, 2003: A Rocky mountain storm. Part II: The forest blowdown over the west slope of the northern Colorado mountains—Observations, analysis, and modeling. *Wea. Forecasting*, **18**, 662–674, https://doi.org/10.1175/1520-0434(2003)018<0662:ARMSPI>2.0.CO;2.

Mitchell, D. L., R. Zhang, and R. L. Pitter, 1990: Mass-dimensional relationships for ice particles and the influence of riming on snowfall rates. *J. Appl. Meteor.*, **29**, 153–163, https://doi.org/10.1175/1520-0450(1990)029<0153:MDRFIP>2.0.CO;2.

Morrison, H., and J. A. Milbrandt, 2015: Parameterization of cloud microphysics based on the prediction of bulk ice particle properties. Part I: Scheme description and idealized tests. *J. Atmos. Sci.*, **72**, 287–311, https://doi.org/10.1175/JAS-D-14-0065.1.

——, G. Thompson, and V. Tatarskii, 2009: Impact of cloud microphysics on the development of trailing stratiform precipitation in a simulated squall line: Comparison of one- and two-moment schemes. *Mon. Wea. Rev.*, **137**, 991–1007, https://doi.org/10.1175/2008MWR2556.1.

Murray, B. J., D. O'Sullivan, J. D. Atkinson, and M. E. Webb, 2012: Ice nucleation by particles immersed in supercooled cloud droplets. *Chem. Soc. Rev.*, **41**, 6519–6554, https://doi.org/10.1039/c2cs35200a.

Naeger, A. R., B. A. Colle, N. Zhou, and A. Molthan, 2020: Evaluating warm and cold rain processes in cloud microphysical schemes using OLYMPEX field measurements. *Mon. Wea. Rev.*, **148**, 2163–2190, https://doi.org/10.1175/MWR-D-19-0092.1.

Nakaya, U., 1954: *Snow Crystals, Natural and Artificial*. Harvard University Press, 510 pp.

Ono, A., 1970: Growth mode of ice crystals in natural clouds. *J. Atmos. Sci.*, **27**, 649–658, https://doi.org/10.1175/1520-0469(1970)027<0649:GMOICI>2.0.CO;2.

Poulos, G. S., D. A. Wesley, J. S. Snook, and M. P. Meyers, 2002: A Rocky mountain storm. Part I: The blizzard—Kinematic evolution and the potential for high-resolution numerical forecasting of snowfall. *Wea. Forecasting*, **17**, 955–970, https://doi.org/10.1175/1520-0434(2002)017<0955:ARMSPI>2.0.CO;2.

Rangwala, I., and J. R. Miller, 2012: Climate change in mountains: A review of elevation-dependent warming and its possible causes. *Climatic Change*, **114**, 527–547, https://doi.org/10.1007/s10584-012-0419-3.

Saleeby, S. M., and W. R. Cotton, 2004: Simulations of the North American monsoon system. Part I: Model analysis of the 1993 monsoon season. *J. Climate*, **17**, 1997–2018, https://doi.org/10.1175/1520-0442(2004)017<1997:SOTNAM>2.0.CO;2.

——, and ——, 2005: A large-droplet mode and prognostic number concentration of cloud droplets in the Colorado State University Regional Atmospheric Modeling System (RAMS). Part II: Sensitivity to a Colorado winter snowfall event. *J. Appl. Meteor.*, **44**, 1912–1929, https://doi.org/10.1175/JAM2312.1.

——, and S. C. van den Heever, 2013: Developments in the CSU–RAMS aerosol model: Emissions, nucleation, regeneration, deposition, and radiation. *J. Appl. Meteor. Climatol.*, **52**, 2601–2622, https://doi.org/10.1175/JAMC-D-12-0312.1.

Takahashi, T., and N. Fukuta, 1988: Supercooled cloud tunnel studies on the growth of snow crystals between −4 and −20°C. *J. Meteor. Soc. Japan*, **66**, 841–855, https://doi.org/10.2151/jmsj1965.66.6_841.

——, T. Endoh, G. Wakahama, and N. Fukuta, 1991: Vapor diffusional growth of free-falling snow crystals between −3 and −23°C. *J. Meteor. Soc. Japan*, **69**, 15–30, https://doi.org/10.2151/jmsj1965.69.1_15.

Thompson, G., R. M. Rasmussen, and K. Manning, 2004: Explicit forecasts of winter precipitation using an improved bulk microphysics scheme. Part I: Description and sensitivity analysis. *Mon. Wea. Rev.*, **132**, 519–542, https://doi.org/10.1175/1520-0493(2004)132<0519:EFOWPU>2.0.CO;2.

——, P. R. Field, R. M. Rasmussen, and W. D. Hall, 2008: Explicit forecasts of winter precipitation using an improved bulk microphysics scheme. Part II: Implementation of a new snow parameterization. *Mon. Wea. Rev.*, **136**, 5095–5115, https://doi.org/10.1175/2008MWR2387.1.

Tsai, T.-C., and J.-P. Chen, 2020: Multimoment ice bulk microphysics scheme with consideration for particle shape and apparent density. Part I: Methodology and idealized simulation. *J. Atmos. Sci.*, **77**, 1821–1850, https://doi.org/10.1175/JAS-D-19-0125.1.

Walko, R. L., W. R. Cotton, M. P. Meyers, and J. Y. Harrington, 1995: New RAMS cloud microphysics parameterization. Part I: The single-moment scheme. *Atmos. Res.*, **38**, 29–62, https://doi.org/10.1016/0169-8095(94)00087-T.

Wegener, A., 1911: *Thermodynamik der Atmosphäre*. J. A. Barth, 331 pp.

Woods, C. P., M. T. Stoelinga, and J. D. Locatelli, 2007: The IMPROVE-1 storm of 1–2 February 2001. Part III: Sensitivity of a mesoscale model simulation to the representation of snow particle types and testing of a bulk microphysical scheme with snow habit prediction. *J. Atmos. Sci.*, **64**, 3927–3948, https://doi.org/10.1175/2007JAS2239.1.

Yang, P., and K.-N. Liou, 1998: Single-scattering properties of complex ice crystals in terrestrial atmosphere. *Contrib. Atmos. Phys.*, **71**, 223–248.